Failure of rammed earth walls: from observations to quantifications

Tan Trung Bui, Quoc-Bao Bui, Ali Limam, Sandrine Maximilien

Failure of rammed earth walls: from observations to quantifications

T.-T. Bui [1], Q.-B. Bui [2], A. Limam [1], S. Maximilien [3]

[1] *INSA de Lyon, LGCIE, 69621 Villeurbanne, France.*

[2] *Université de Savoie, POLYTECH Annecy-Chambéry, LOCIE - UMR5271, 73376 Le Bourget du Lac, France.*

[3] *INSA de Lyon, MATEIS, 69621 Villeurbanne, France*

** Corresponding author:*

Email:Quoc-Bao.BUI@univ-savoie.fr

Abstract

Nowadays, rammed earth construction is attracting renewed interest throughout the world thanks to its "green" characteristics in the context of sustainable development. Firstly, using a local material (soil on site or near the site), rammed earth constructions have very low embodied energy. Secondly, rammed earth houses have an attractive appearance and present advantageous living comfort due to substantial thermal inertia and the “natural regulator of moisture” of rammed earth walls. This is why several research studies have been carried out recently to study the mechanical and thermal characteristics of rammed earth. However, to our knowledge, there are not yet sufficient studies on the tensile strength and the shear strength of rammed earth. The tensile strength of rammed earth is neglected in general due to its very low value, but in extreme conditions (e.g., seismic conditions), knowing the tensile strength is necessary for structural design. Moreover, the shear strength is required in many cases to check the local failure of rammed earth quickly, which has been observed in old structures (especially those submitted to concentrated loads).

This paper presents experimental results on tensile strengths and the Poisson ratio of rammed earth specimens. Local failure tests were also conducted on 1 m × 1 m × 0.3 m wallettes manufactured in the laboratory. The shear strength was then identified using a simple method based on compressive strength, tensile strength and Mohr’s circle theory. The approach proposed was validated by tests on the wallettes. Finite Element (FE) modeling was also carried out to confirm the results. Last, the method presented was validated for stabilized rammed earth lintels presented in the literature.

Keywords: rammed earth, tensile strength, shear strength, failure.

1 Introduction

Rammed earth materials are ideally sandy-clayey gravels. The materials are prepared to their optimum moisture content and compacted inside a temporary formwork to form walls. The earth composition varies greatly and always contains clay but should not include any organic components. Clay acts as the binder between the grains, a mixture of silt, sand, and gravel up to a few centimeters in diameter. Compaction is undertaken on material prepared to its optimum moisture that provides the highest dry density for the given compactive energy (Bui *et al.* 2009b). The rammed earth wall is composed of several layers of earth. The earth is poured loose in layers about 10–15 cm thick into a timber or metal formwork, which is then rammed with a rammer (manual or pneumatic). After compaction, the thickness of each layer is typically 6–10 cm. The procedure is repeated until completion of the wall. A detailed presentation of rammed earth construction can be found in Walker *et al.* (2005).

For traditional rammed earth construction, referred to as "rammed earth" (RE) or "unstabilized rammed earth," the only binder is clay. Other binders can also be added such as cement or hydraulic or calcium lime, were added. This is often called "stabilized rammed earth" (SRE). The main advantage of stabilization is the increase in durability and mechanical performance. However, stabilization increases the construction cost and environmental impact.

Rammed earth is the focus of scientific research for two main reasons. Firstly, in the context of sustainable building, the modern interest in earth as a building material is largely derived from its low embodied energy, both for unstabilized rammed earth (Morel *et al.* 2001) and stabilized rammed earth (Reddy and Kumar 2010), and also because the material has good natural moisture buffering from indoor environments (Allinson and Hall 2010). Secondly, the heritage of rammed earth buildings in Europe and the world is still important (Fodde 2009, Bui *et al.* 2009a). Maintaining this heritage needs scientific knowledge to assess appropriate renovations.

Several research studies have recently been conducted to study the characteristics of rammed earth: durability and sensitivity to water (Bui *et al.* 2009a, Hall and Djerbib 2004a), thermal properties (Taylor et al. 2008, Taylor and Luther 2004), living comfort (Paul and Taylor 2008), mechanical characteristics in compression (Bui *et al.* 2009b, Bui and Morel 2009, Maniatidis and Walker 2008, Hall and Djerbib 2004b, Jaquin *et al.* 2009); pullout strength (Walker *et al.* 2001), and dynamic characteristics (Bui *et al.* 2011).

However, there are not yet sufficient studies on the tensile strength and the shear strength of rammed earth (Cheah *et al.* 2012). The tensile strength of rammed earth is neglected in general due to its very low value, but in extreme conditions (e.g. seismic), knowing tensile strength is necessary for the structural design (Gomes *et al.* 2011). Shear strength is also required in many cases to check the punching strength of rammed earth walls quickly (Fig. 1), such as beams directly placed on a rammed earth wall (roof beams, lintel beams; Ciancio and Robinson 2011) and vertical ties in anti-seismic devices (Hamilton *et al.* 2006).

This paper presents the experimental results on tensile strengths and the Poisson ratio of rammed earth. The shear strength is also identified using a simple method based on compressive strength, tensile strength, and Mohr's circle theory. The approach proposed was then validated by the tests on the (1 m × 1 m × 0.3 m) walls manufactured in the laboratory. FE modeling taking account the non-linear behavior of RE material was also conducted. The material studied in this paper is unstabilised rammed earth but the presented method is also applicable in the case of stabilized rammed earth.

Figure 1: Typical failure of an old rammed earth wall in France.

2 Manufacture of specimens

2.1 Soils

Three different soils were used in this study (Table 1). These soils were taken directly from the RE building sites. The soils have the clay contents convenient for RE manufacture (5–10%, Walker *et al.* 2005).

Table 1: Soils used in this study

Soil	Clay (by weight)	Silt	Sand	Gravel
A	10%	25%	18%	47%
B	5%	30%	49%	16%
C	8%	34%	8%	50%

2.2 Different types of specimen

The representativeness of specimens manufactured in laboratory was discussed in a pevious study (Bui *et al.* 2009b). In the present study, to identify several parameters that are useful for numerical and analytical models that will be presented in this paper, several tests in both directions with several types of specimen are necessary: cylindrical specimens for tests determining the Poisson ratio and the tensile strength within earthen layers (Brazilian test), prismatic specimens for compression tests, and wallettes for tests identifying the behavior and failure mode of RE walls under concentrated loading. The choice of each type of specimen will be explained in the corresponding section.

2.3 Cylindrical specimen manufacturing

To determine the tensile strength using the Brazilian test and measure the Poisson ratio, cylindrical specimens were needed. Extensometers were used on prismatic specimens without success because a square section did not enable homogeneous movements of the elastic wires that connected the extensometers (for greater detail, see section 3.1)

The automatic Proctor machine was adopted (Figure 2). The standard mold of the Proctor test was replaced by a mold 16 cm in diameter and 32 cm high. To obtain the dry density of *in-situ* rammed earth material (~1920 kg/m^3; Bui *et al.* 2009b), a series of preliminary tests were conducted to determine the manufacturing water content and the amount of soil to be poured into the mold for each layer. An 11% moisture content was chosen as the compaction moisture content and 2.2 kg of moist soil was weighed out for each layer. Each layer received the Proctor energy (E = 0.6 kJ/dm^3). There were six compaction layers in each specimen prepared. The final height of the cylinder after the release was about 30 cm. Prior to mixing, the soil was sieved through a 2-cm screen.

Figure 2: Automatic Proctor machine and modified mold.

After the compaction process, the specimens were removed from the mould. The bottom surface of the cylinder, since it was in contact with the bottom side of the mold during compaction, was smooth and did not require any further treatment before strength testing. However, the more uneven upper surface was capped with a mortar (2 lime: 3 sand by weight) to provide a flat smooth surface parallel with the bottom side. During drying, the specimen was left in the ambiant atmosphere.

2.4 Manufacture of prismatic specimens

To ensure a faithful representation of the in-situ wall material, the manufacturing mode and material used for laboratory specimens should be as identical as possible to those used for the rammed earth houses. Therefore the earth was taken from the construction site of a rammed earth house (soil B). The manufacturing water content and the compaction energy in the laboratory were the same as on site. The manufacturing water content was about 10%.

The dimensions of specimens tested in the direction perpendicular to the layers were 40cm x 40cm x 70cm, with nine layers (Bui *et al.* 2009a). The specimens tested in the direction parallel to the layers were composed of only three layers. The specimen dimensions are 40 cm × 40 cm and roughly 20 cm high. The last layer is given special attention during compaction to obtain a surface that is as flat as possible. To achieve a slenderness ratio of 2, the specimens are then cut with a table saw. Three specimens measuring (40 × 40 × 20) cm^3 were manufactured, which provided six specimens (20 × 20 × 40) cm^3 for testing in the parallel direction. Since the specimen is tested in the direction parallel to the layers, surfacing is not necessary, because the two surfaces that were in contact with the formwork are sufficiently flat.

A section formwork measuring 40×40 cm^2 was chosen for the following reasons: a larger section makes it impossible to put specimens on the press to test in the direction perpendicular to the layers. In addition, a

smaller cross-section makes it impossible to manufacture representative specimens tested in the direction parallel with the layers. Indeed, for compression tests in the direction parallel to the layers, the specimen must have at least three layers because the last layer is less compacted and consequently less representative (Bui and Morel 2009). Therefore, the specimen had to measure at least 20 cm for each side. More details on the manufacture of representative specimens can be found in Bui *et al.* (2009a).

2.5 Manufacture of wallettes

In order to study the general behavior of RE walls and especially the walls subjected to concentrated loads, two walls measuring (100 × 100 × 30) cm^3 were made with soil C. The thickness of each layer after compaction was 14–15 cm. Surfacing was provided by a layer of mortar.

3 Characterization on "small" specimens

3.1 Compression in the direction perpendicular to layers

The cylindrical specimens with 16cm diameter and 30cm height were tested in compression between two hardened steel plates. Three cylinders were tested for each series. To measure service strains, extensometers were placed in the central half of the cylinders to minimize end effects on measured performance. To determine the Poisson ratio, lateral strain measurements, as well as vertical measurements, were taken. Figure 3 shows the configuration of a uniaxial compression strength test: extensometers measured the longitudinal strains and LVDT sensors measured lateral displacements, which helps calculate the lateral strains.

For each test, three extensometers and three LVDT sensors, fixed at an interval of 120° on the radial plan, were used to verify the repeatability of the results. An extensometer measures the strain between two points: one point at the center of a layer and the other point at the center of the upper layer. The distance between two points of the extensometer is 6.2 cm, while the thickness of a layer of the specimen is about 5 cm. The cylinders were loaded by displacement control at a constant rate of 0.1 mm/min until failure.

For the soil C specimens (wallette soil), the compressive strength, the Young modulus and the Poisson's ratio measured were 1.9 ± 0.2 MPa, 500 ± 40 MPa, and 0.22± 0.01, respectively. The results of other specimens will be presented in the following section. More information about the characterization on cylindrical specimens can be found in Bui *et al.* (2013).

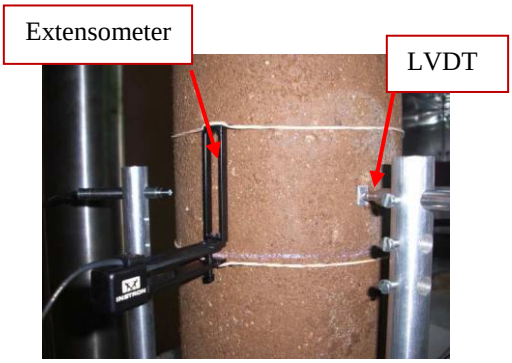

Figure 3: Set-up to measure the Poisson ratio.

3.2 Compression in the direction parallel to layers

The compression tests in the parallel direction of the layers were *a priori* done a nonhomogenous material (Fig. 4a). Firstly, the stress was not uniform in the specimen during the test due to the heterogeneity of the dry density within a layer (which increased from the bottom to the up of layer). So the stress was discontinuous from one layer to another. Therefore, the determined stress was an average value (the load applied by the press divided by the section of the specimen). Secondly, layer separation occurred fairly early during the test, notably the first crack in the last layer, meaning that the specimen was no longer a continuous medium. However, these separations did not seem to significantly alter the specimen's mechanical capacities, since each layer continued to support the load alone. There was no change in slope even after the abrupt loss of adhesion due to the separation (Fig. 4b). During the test, the first crack appeared fairly early, due to the separation of the last manufacturing layer (Fig. 4a). This phenomenon has already been discussed in Bui and Morel (2009). The complete failure of the specimen occurred when the third vertical crack appeared. It corresponded to the maximum extension of the material (the strain corresponds to the maximal stress) and to the internal failure within a layer leading to the failure of the entire specimen. The results will be discussed in section 3.3.2 and will be used to identify tensile strength at the interfaces between layers.

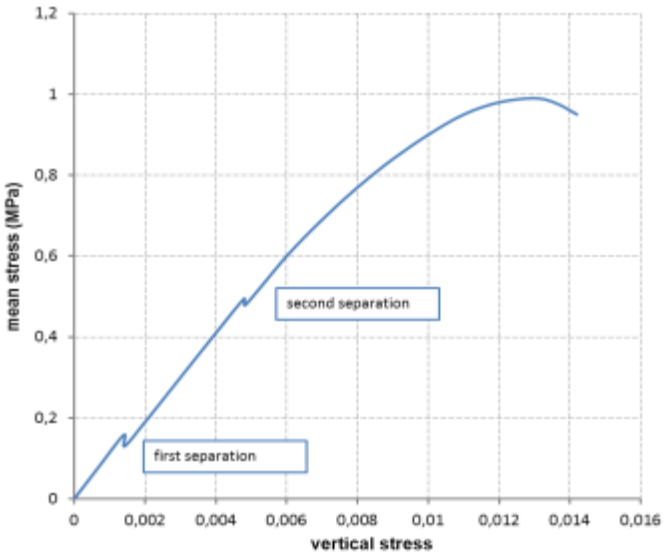

(a) (b)

Figure 4: Uniaxial compression test in the direction parallel to the layers

3.3 Tensile strength

Since RE is a superposition of earth layers, it is necessary to distinguish two tensile strengths: the tensile strength in earth layers and the tensile strength at the interfaces of earth layers (Fig. 4a).

3.3.1 Tensile strength within rammed earth layers

Within a RE layer, the mechanical behaviors are similar in the directions parallel and perpendicular to the layers (Bui and Morel 2009). Therefore, it is supposed that the tensile strengths within a layer are also similar in two directions.

To determinate the tensile strength within earth layers, the Brazilian test was used (Fig. 5). The synthesis of the results is illustrated in Fig. 6.

Figure 5 Brazilian test to determine the tensile strength

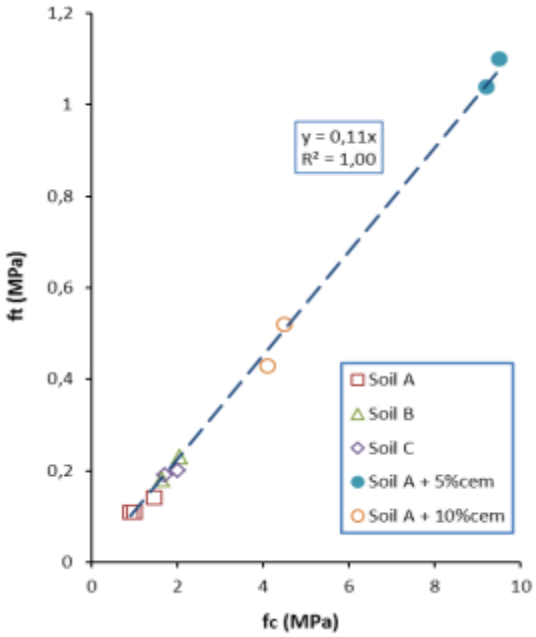

Figure 6: Relationship between the compressive strength and the tensile strength in earth layers.

To apply the analytical method that will be presented in section 4.5 for stabilized rammed earth, soil A was also stabilized at 5% and 10% by cement (by weight). The results of these stabilized specimens are also presented in Fig. 6.

Figure 6 presents the experimental relationship between the compressive strength and the tensile strength within the layers of the tested specimens. From this figure, the tensile strength within layers (f_t) can be expressed by: $f_t=0.11\ f_c$ where f_c is the compressive strength. This expression can be simplified: $f_t=0.1\ f_c$.

3.3.2 Tensile strength at interfaces between layers

To assess the difference between the tensile strength in layers and the tensile strength at interfaces between layers (excluding the last layer), the latter was identified.

Call x and z the directions perpendicular and parallel to the layers, respectively;

Lateral strain in the direction parallel to layers: $\varepsilon_{xx} = - \nu_{xx}\, \varepsilon_{zz} = - \nu_{xx}\, \sigma_{zz} / E_{zz}$ (1)

Thus, lateral stress in the direction parallel to layers: $\sigma_{xx} = E_{xx}\, \varepsilon_{xx} = - E_{xx}\, \nu_{xx}\, \sigma_{zz} / E_{zz}$ (2)

Bui and Morel (2009) showed that the Young moduli in both directions were similar: $E_{xx} \cong E_{zz}$

$\Rightarrow$ $\sigma_{xx} = - \nu_{xx}\, \sigma_{zz}$ (3)

Following the results of tests in the direction parallel to layers, separation of the second layer was about 50% of the compressive strength in this direction ($\sigma_{zz,\ separation} \cong 0.5\ \sigma_{zz\ max}$; Fig. 4b). The Poisson's ratio measured was 0.22 (more information can be found in Bui *et al.* 2013).

Replace these parameters in (3), it is obtained that in the direction parallel to the layers, the normal stress immediately before the separation:

$\Rightarrow \quad \sigma_{xx} = -0.22 \times 0.5\ \sigma_{xx,\ max} = -0.11\ f_c$

This result shows that the tensile strength at layer interfaces (excluding the last layer) is similar to the tensile strength within the layers. Because of the layer's superposition of RE material, this result is quite surprising but shows that the assumption of an isotropic material is totally acceptable for RE. It is important to note that this result was calculated for the separation at approximately 50% (observed on the stress-strain relationship), but this separation may initiate earlier inside the specimen. Another method may be a flexural test on a RE beam, in perpendicular or parallel to the layers.

The result of this section is simply to evaluate the anisotropy of RE material in traction; it has no influence on the results of the following sections of this paper.

4 Tests on the wallettes

4.1 Test procedure

A quasi-static loading was applied by a hydraulic press (capacity, 2000 kN) on a (30×30) cm^2 surface at the middle of the wall (Figure 7). The wall displacements were measured using five displacement sensors (LVDT) positioned on the wall (two vertical sensors, two lateral sensors, and an out-of-plane sensor). In addition, the 3D-image-correlation technique with a stereo vision system was applied to a wallette face, making it possible to record deformations of this surface in three directions. Two 4-megapixel cameras (ALLIED Vision Technologies) were used for image acquisition. First, the investigated side was coated by a white pure hydrated lime and then black speckles were painted on this white background. The 3D displacements were measured by recording the movements of these speckles. Then the strains were calculated automatically from these displacements using Vic-3D software.

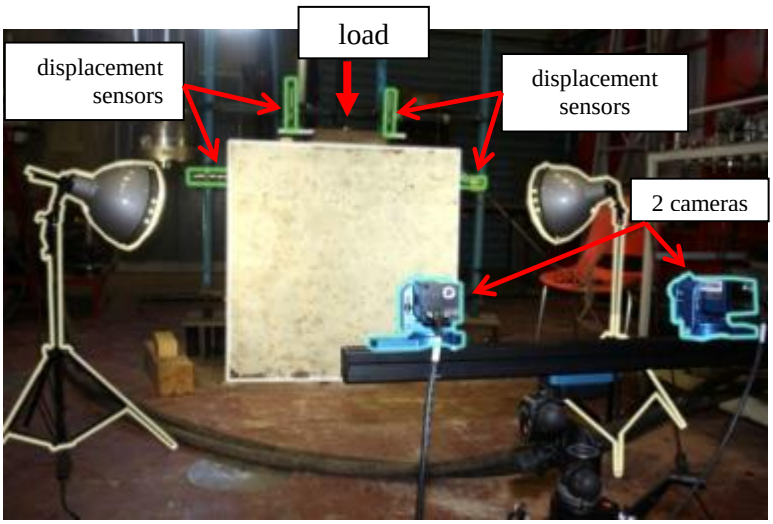

Figure 7: Experimentation on a wallette

The tests were carried out 148 and 155 days after the wallettes' manufacture for the first and second wallette, respectively to assure that the wallets' water content was stable and the wallets could be considered as "dry" (Bui *et al.* 2009b). The wallettes' water content was determined after the tests and were 1.8 ± 0.2%.

4.2 Results

Figure 8 presents the load–displacement relationships obtained for two wallettes. These two curves are similar, which shows a repeatability of results. The behavior was quasi-linear up to 42 and 45 kN, respectively, for the first and second wallettes. Then a decrease in the slope was observed, corresponding to the appearance of the first cracks in the wallettes. The mean failure load of the two wallettes reached 112 kN, which corresponds to a vertical displacement about 4.5 mm from the wallette's central point. The third phase was a post-peak behavior, which presents a substantial drop in the slope.

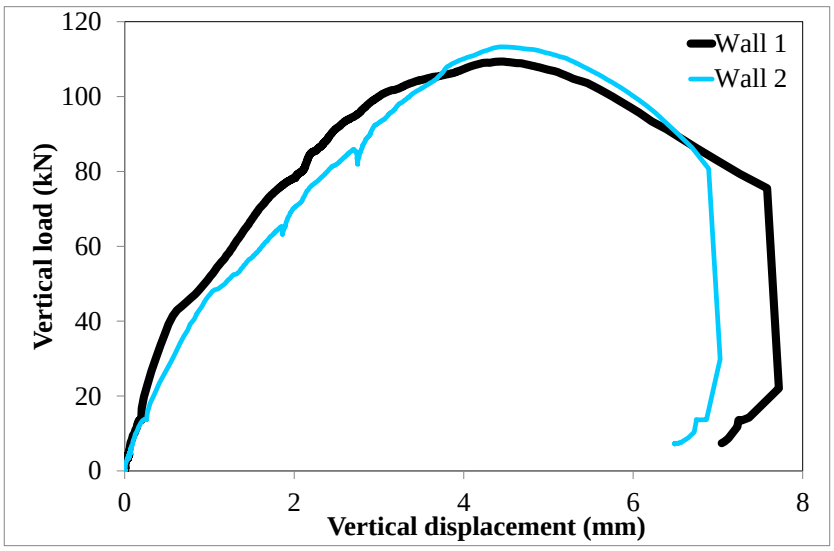

Figure 8: Load–displacement relationship of two wallettes.

Monitoring the crack propagation was recorded by the image correlation. Synchronization between the stereovision system and the load and displacement sensors identified the behavior of the wallettes and crack appearance (Figure 9). The cracks were identified by observing the horizontal strains ε_{xx} of the wallette face. At the beginning of the second phase (post-elastic phase, point P1 on Figure 9), a vertical crack was observed. Then this vertical crack continued to develop and other vertical cracks appeared in the central part (points P2 and P3 in Figure 9). When the post-peak phase began (point P4 in Figure 9), inclined cracks appeared, which propagated to two corners of the wallette. These inclined cracks seem to have been influenced by the friction between the wallette and the metallic base.

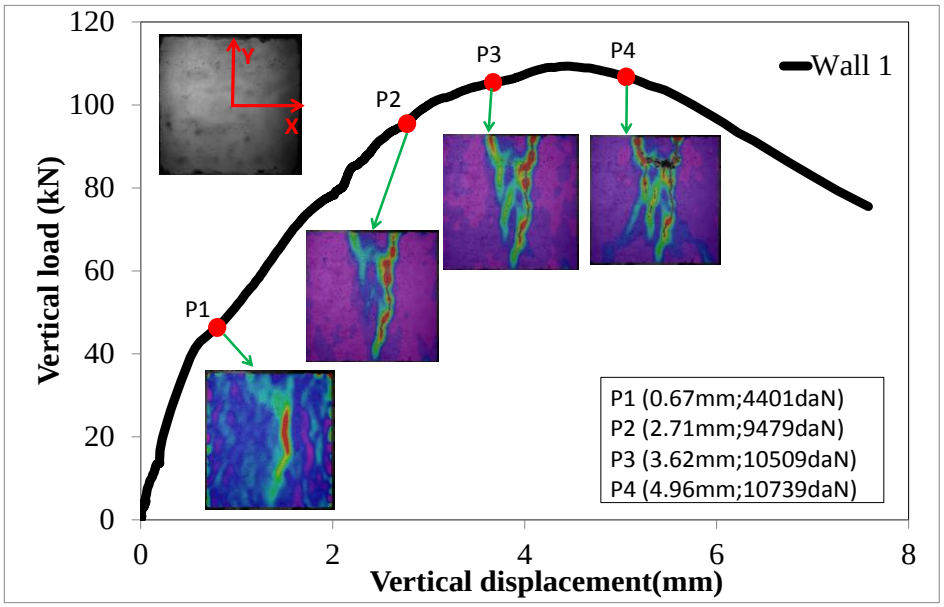

Figure 9: Crack development on wallette 1.

Two types of cracking were observed: vertical cracks which appeared in the central part and inclined cracks at the corners. These cracks crossed the compacted earth layers, and there was no crack bifurcation at the layer interfaces. This means that the cracks were not influenced by the layer's superposition, so the hypothesis of a homogeneous material was acceptable in this case.

(a) (b)

Figure 10: Failure modes of the wallettes: (a) Wallette 1; (b) Wallette 2.

The experiment showed that the wallette zone that was under loading underwent failures and greater settlement than other zones (

Figure 10). A fracture surface developed between the loaded zone and the neighbor unloaded zone because of a differential settlement (Figure 11). This fracture surface was quasi-vertical and so different from those in reinforced concrete structures where the fracture was about 45° from the horizontal plane. In concrete constructions, several empirical formulas are proposed to determine the shear strength (Eurocode 2), which is a function of the compressive strength. For RE material, to study the behavior of a concentrated load, shear strength must also be determined.

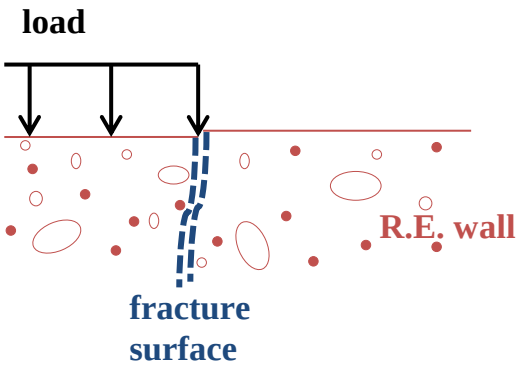

Figure 11: Fracture surface

Following Morh-Colomb theory, the shear strength is a function of cohesion, normal stress and friction angle. The material's cohesion can be quickly determined by applying the theory of Mohr's circles for compressive and tensile strengths. Following Morhr's circles and using the results presented in the first part of this paper ($f_t=0.11f_c$), cohesion and friction angle were identified: $c=0.14f_c$ and $\varphi=51°$. This result means that for REs whose compressive strength is about 1–3 MPa, the cohesion is about 0.14–0.42 MPa. These values are coherent with the value found in the literature. Indeed, in Jaquin *et al.* (2006), a cohesion of 0.15 MPa was identified for their specimens using a numerical model; in Cheah *et al.* (2012), cohesion and friction angle of stabilised rammed earth were measured that were 45-56° and 280-760kPa respectively.

4.3 Discussion

For old RE walls that underwent concentrated loads, vertical cracks often appeared at the boundary between the loaded zone and the unloaded zone, which resemble a fracture surface because of differential sliding.

The mean compressive strength of cylindrical specimens manufactured from the same soil as the wallettes was 1.9 MPa. If this strength was applied, the wallettes can resist a load of 171 kN (1900 kPa × 0.3 m × 0.3 m), which should overestimate the result (the experimental result was 112 kN).

In the experimental failure state, the maximal normal stress in the wallette was 1.22 MPa, which was the normal stress of the points under the loaded zone. It is well known in soil mechanics that away from this zone, stress decreases. If the above theoretical formula ($\nu=0.14f_c$) was applied, the theoretical cohesion at the loaded zone was 0.17 MPa.

By assuming the two failure surfaces were vertical at the extremities of the loaded zone (each vertical surface was 1 m high × 0.3 m wide), the strength of the wallettes should be 124 kN. This result was close to the experimental result, which was approximately 112 kN (Table 2 2). The difference could result on one hand from the failure surface not being perfectly vertical; the angle θ can vary from 0° to 10°. On the other hand, slenderness of the walls was greater than 2 that may induce the buckling which could decrease the experimental results.

Table 2 : Comparison between the experimental and theoretical failure loads

Experimental failure load F_{exp}	112 kN
Vertical compressive stress f_c	1.22 MPa
Theoretical cohesion ($\nu_{theo} = 0.14f_c$)	0.17 MPa
Theoretical failure load F_{theo}	124 kN

It is known that the representativeness of cylindrical specimens is limited (Bui *et al.* 2009b, Ciancio and Gibbings 2012); it is possible that the "true" compressive strength of the wallettes was lower than the cylindrical specimens. To reassess the role of cohesion on the bearing capacity of RE walls under concentrated loads, a numerical study was conducted, which will be presented in the following section.

4.4 Finite Element modeling

The wallettes were modeled using the advanced Finite Elements (FE) CASTEM code in which the complex behaviors of materials were taken into account: nonlinearity, cracking and damage. The Mazars model (Mazars 1986) was used. This is an isotropic nonlinear damage model and is frequently used for modeling damage in concrete. This model is based on damage mechanics, so it can identify the decrease in stiffness caused by the appearance of micro-cracks in the material. It is based on the scalar internal variable *D*, which describes the damage in tensile or compressive loadings (Lemaitre 1996). The progression of damage is distinguished by the sign of solicitation and is modeled by two scalar internal variables in tensile (D_t) and compressive damage (D_c).

In the model, the wallette was considered homogenous and isotropic. This hypothesis was proved acceptable in a previous study (Bui *et al.* 2009b). The modeling was in 2D (plane stress). The QUA4 elements (20 mm × 20 mm) with four Gaussian points were used. The Young modulus and the Poisson's ratio were 500 MPa and 0.22, respectively, according to experimental results on cylindrical specimens. Two models were tested: in the first, a compressive strength of 1.9 MPa was used and in the second a compressive strength of 1.3 MPa was used. Shear strength of 0.18 MPa was used for both models.

The numerical and experimental results are compared in Fig. 12. The initial stiffness obtained by the FE model was identical to the experimental result (Fig. 12a); this shows that the Young modulus used was correct. The numerical model could not reproduce the second phase of the walls' behavior when the cracking began and the stiffness decreased; this shows the limit of the used damage model. Indeed the Mazars model

is well known that it can reproduce the maximal load (by reproducing the damage energy) but it can not reproduce the form of the behavior curve. Fig. 12b presents the evolution of dissipated energies that shows that the numerical model captured well the damage energy (at 4.5-mm vertical displacement).

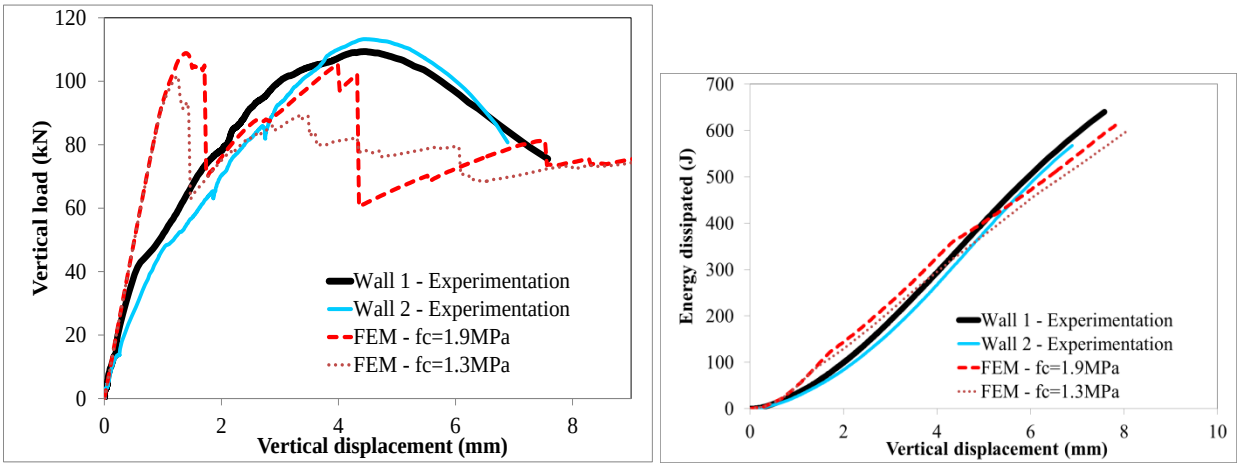

a) b)

Figure 12 Comparison of the numerical and experimental results.

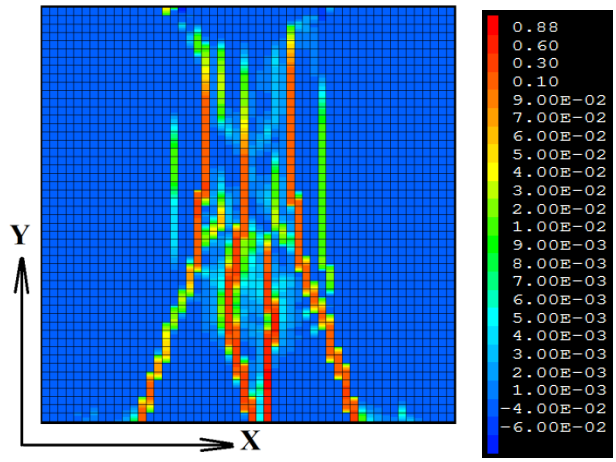

Figure 13: Horizontal strains ε_{xx} in the numerical model (at a 9mm vertical displacement).

The failure modes of the numerical model were also similar to the experimentation (Figure 13): firstly, the central vertical cracks appeared and then the inclined cracks propagated to the bottom corners of the wallette. The numerical maximal loads were 110 kN and 103 kN, respectively, for 1.9 and 1.3 MPa of compressive strength. These numerical results were close to the experimental results: the difference did not exceed 10%. In these models, the compressive strength was varied but the shear strength was not modified. The numerical results show that the compressive strength was not a primary parameter in this case because a 50% increase

in compressive strength leads to only a 6% increase in the wallette's maximal load. The stress concentration played an important role in this case and therefore the shear strength was the most important parameter.

4.5 Shear strength on deep beams

Ciancio and Robinson (2011) used the "strut-and-tie" method to model lintels in SREs reinforced by lower longitudinal metallic rods. The "strut-and-tie" method worked well on most of the lintels studied; however, there were four lintels whose their failure mode and strength the authors could not explain. Indeed, these lintels were cracked due to the stress concentration (Figure 14) that was shown in the present study. This section will check whether the criteria based on shear strength reproduces the experimental results in the Ciancio and Robinson study.

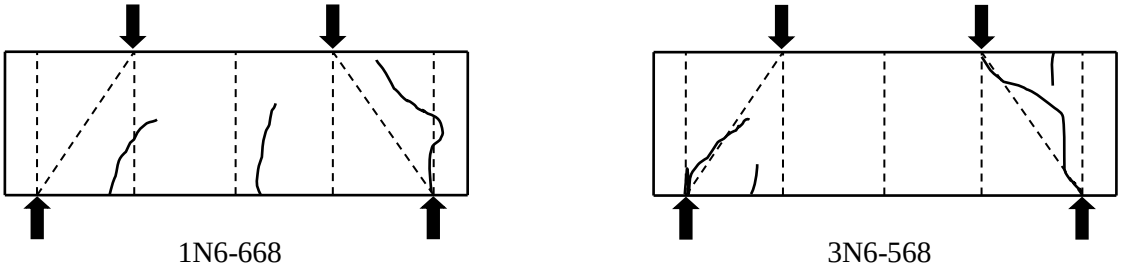

Figure 14: Failure of the four lintels in the Ciancio and Robinson (2011) study

In the Ciancio and Robinson (2011) study, there were three values of compressive strength:

- Tests on cylindrical specimens that were manufactured in the cylindrical molds (D 10 cm × H 20 cm),
- Tests on cylindrical specimens (D 8 cm × H 16 cm), which were cored from the wallettes,
- Values recalculated from the maximal load obtained after tests on the lintels.

Among these three values, the values of the specimens manufactured in the molds are often overestimated (Bui *et al.* 2009b, Ciancio and Gibbings 2012). On the other hand, the tests on cored specimens usually give underestimated results because the specimen's microstructure is changed due to coring (Bui *et al.* 2007, Ciancio and Gibbings 2012). The recalculated values were between these two cases and therefore appear to be the best estimate. It is interesting to note that for SREs, the failure angle can also vary from 0° to 20° relative to the vertical plane.

The results obtained by the cohesion criteria and the experimental results are compared in Table 3. The differences are relatively small (up to 10% overestimation), which proves that the approach using cohesion can explain the experimental results. In practice, the formula $f_{sh} = 0.1f_c$ can be suggested.

Table 3 Comparison between the experimental results obtained by Ciancio and Robinson (2011) and the theoretical results obtained by the cohesion-based criterion.

Beam	Specimens	f_c (Mpa)	f_{sh} (Mpa)	$P_{theo.}$ (kN)	$P_{exp.}$ (kN)	P_{theo}/P_{exp}
	rammed cylinder	14.8	2.07	120.9	119.4	1.01
3N6-568	cored cylinder	9	1.26	73.5	119.4	0.62
	calculated	15.9	2.23	129,9	119.4	**1.09**
	rammed cylinder	17.5	2.45	135.4	100.4	1.35
2N6-568	cored cylinder	11	1.54	85.1	100.4	0.85
	calculated	13.4	1.88	103.7	100.4	**1.03**
1N6-468	rammed cylinder	7.5	1.05	63.0	46.8	1.35
	calculated	6,2	0.87	52.1	46.8	**1.11**
1N6-668	rammed cylinder	4	0.56	30.2	39.3	0.,77
	calculated	5.2	0.73	39.2	39.3	**1.00**

5 Conclusion and prospects

This paper contributes data for RE structures subjected to specific loads: seismic loads and concentrated loads. For seismic loads, a series of experiments were conducted to determine the tensile strength of RE material. A relationship between the tensile and the compressive strengths was identified ($f_t=0.11f_c$). It was surprising that the tensile strength at the layer's interfaces was similar to that within the layers, but this result confirms that the isotropic hypothesis is acceptable for RE material.

Concerning the behavior of RE walls under concentrated loads, in addition to the compressive strength criteria, this study suggests that the stress's concentration at the loaded zones should be taken into account. Experiments were conducted on two wallettes subjected to concentrated loads, which demonstrated the vertical failure surfaces due to the differential displacement between the loaded zone and its surrounding unloaded zones. A criterion based on the material's cohesion was proposed to characterize these failure surfaces. Cohesion was identified by Mohr-Coulomb theory. FE modeling, which took into account

nonlinearity and crack development, was used, which confirmed the above results. Then this shear strength-based criterion was applied to a study on SREs, with satisfactory results. The study showed also the limit of the used damage model in the case of RE walls. Further studies are in development to improve the existing model so that it reproduces better the post-elastic phase.

In practice, the tensile strength and the shear strength of RE should be taken equal to 10% of the compressive strength (before being devised by safety factors) because the Mohr-Coulomb criterion may be nonlinear for RE material. If the safety ratio is applied for the compressive strength (which is 1.5 in Eurocode 2), the shear strength will equal 6.7% of the design compressive strength that is similar to recommendations in the New Zealand Standards (1998) which is 7%. Further experiments on other soils should be conducted to validate the approach proposed.

References

Allinson D, Hall M. "Hygrothermal analysis of a stabilised rammed earth test building in the UK", *Energy and Buildings* 42, p. 845–852, 2010.

Bui Q B, Morel J C, Reddy B V V, Ghayad W. "Durability of rammed earth walls exposed for 20 years to natural weathering", *Building and Environment*, vol. 44 (5), p. 912-919, 2009a.

Bui Q B, Morel J C, Hans S, Meunier N. "Compression behaviour of nonindustrial materials in civil engineering by three scale experiments: the case of rammed earth", *Materials and Structures*, vol. 42, N° 8, p. 1101-1116, 2009b.

Bui Q B, Morel J C. "Assessing the anisotropy of rammed earth", *Construction and Building Materials*, 23, pp. 3005-3011, 2009.

Bui Q B, Morel J C, Hans S, Do A-P. "First exploratory study on dynamic characteristics of rammed earth buildings", *Eng. struct.*, p. 3690-3695, 2011

Bui Q B, Hans S, Morel J C. "The compressive strength and pseudo elastic modulus of rammed earth". *International Symposium on Earthen Structures,* Bangalore 08 - 2007, India, p. 217-223, 2007.

Bui Q B, Morel J C, Hans S, Walker P. "Water effects on the mechanical characteristics of rammed earth buildings: a double-edged sword", submitted to *Construction and Building Materials*, 2013.

Cheah J S J, Walker P, Heath A, Morgan T K K B. "Evaluating shear test methods for stabilised rammed earth", *Construction Materials*, Volume 165, Issue CM6, p. 325–334, 2012.

Ciancio D, Robinson S. "Use of the Strut-and-Tie Model in the Analysis of Reinforced Cement-Stabilized Rammed Earth Lintels", *Journal of Materials in Civil Engineering*, Vol. 23, No. 5, May 1, 2011

448 Ciancio D, Gibbings J. “Experimental investigation on the compressive strength of cored and molded
449 cement-stabilized rammed earth specimens”, *Construction and Building Materials*, Volume 28, Issue
450 1, p. 294-304, 2012

451 Eurocode 2. “Design of concrete structures – part 1-1: general rules and rules for buildings”, *NF EN 1992-1-*
452 *1, P 18-711-1*, October 2005.

453 Gomes M I, Lopes M, Brito J. “Seismic resistance of earth construction in Portugal”, *Engineering*
454 *Structures*, Volume 33, Issue 3, Pages 932-941, 2011.

455 Jaquin P A, Augarde C E, Gallipoli D, Toll D G. “The strength of unstabilised rammed earth materials”,
456 *Géotechnique* 59, No. 5, p. 487-490, 2009.

457 Jaquin P A, Augarde C E, Gerrard C M. “Analysis of Historic Rammed Earth construction”, *Structural*
458 *Analysis of Historical Constructions*, New Delhi 2006.

459 Hamilton H R, McBride J, Grill J. "Cyclic Testing of Rammed Earth Walls Containing Post-tensioned
460 Reinforcement", *Earthquake Spectra*, Vol. 22, No. 4, November: 937-959, 2006.

461 Hall M, Djerbib Y. "Rammed earth specimen production: context, recommendations and consistency",
462 *Construction and Building Materials*, 18, p. 281-286, 2004.

463 Hall M, Djerbib Y. "Moisture ingress in rammed earth: Part 1-the effect of soil particle-size distribution on
464 the rate of capillary suction", *Construction and Building Materials*, 18, p. 269-280, 2004.

465 Lemaitre J. “A course on damage mechanics”, 2nd edition, *Springer* 228p., 1996.

466 Maniatidis V, Walker P. "Structural Capacity of Rammed Earth in Compression", *Journal of Materials in*
467 *Civil Engineering*, Vol. 20, No. 3, p. 230-238, 2008.

468 Mazars J. “A description of micro and macro scale damage of concrete structures”, *Engineering Fracture*
469 *Mechanics*, vol. 25, n° 5/6, 1986.

470 Morel J C, Mesbah A, Oggero M and Walker P. "Building houses with local materials: means to drastically
471 reduce the environmental impact of construction", *Building and Environment*, 36, p. 1119-1126, 2001.

472 Paul W L, Taylor P A. "A comparison of occupant comfort and satisfaction between a green building and a
473 conventional building", *Building and Environment*, 43, p. 1858-1870, 2008.

474 Reddy B.V. V., Kumar P. P. “Embodied energy in cement stabilised rammed earth walls”, *Energy and*
475 *Buildings*, Volume 42, Issue 3, Pages 380–385, 2010.

476 Standards NZ. “NZS4297:1998, Engineering design of earth buildings”. *Standards NZ*, Auckland, New
477 Zealand, 1998.

478 Taylor P, Fuller R J, Luther M B. "Energy use and thermal comfort in a rammed earth office building",
479 *Energy and Building*, 40, p. 793-800, 2008.

480 Taylor P, Luther M B. "Evaluating rammed earth walls: a case study", *Solar Energy*, 76, p. 79-84, 2004.

481 Walker P, Dobson S. “Pullout tests on deformed and plain rebars in cement stabilized rammed earth”, *ASCE*
482 *Journal of Materials in Civil Engineering*, 13 (4), p. 291-297, 2001.

483 Walker P, Keable R, Martin J, Maniatidis V. "Rammed earth-Design and construction guidelines", *BRE*
484 *Bookshop*, 2005.